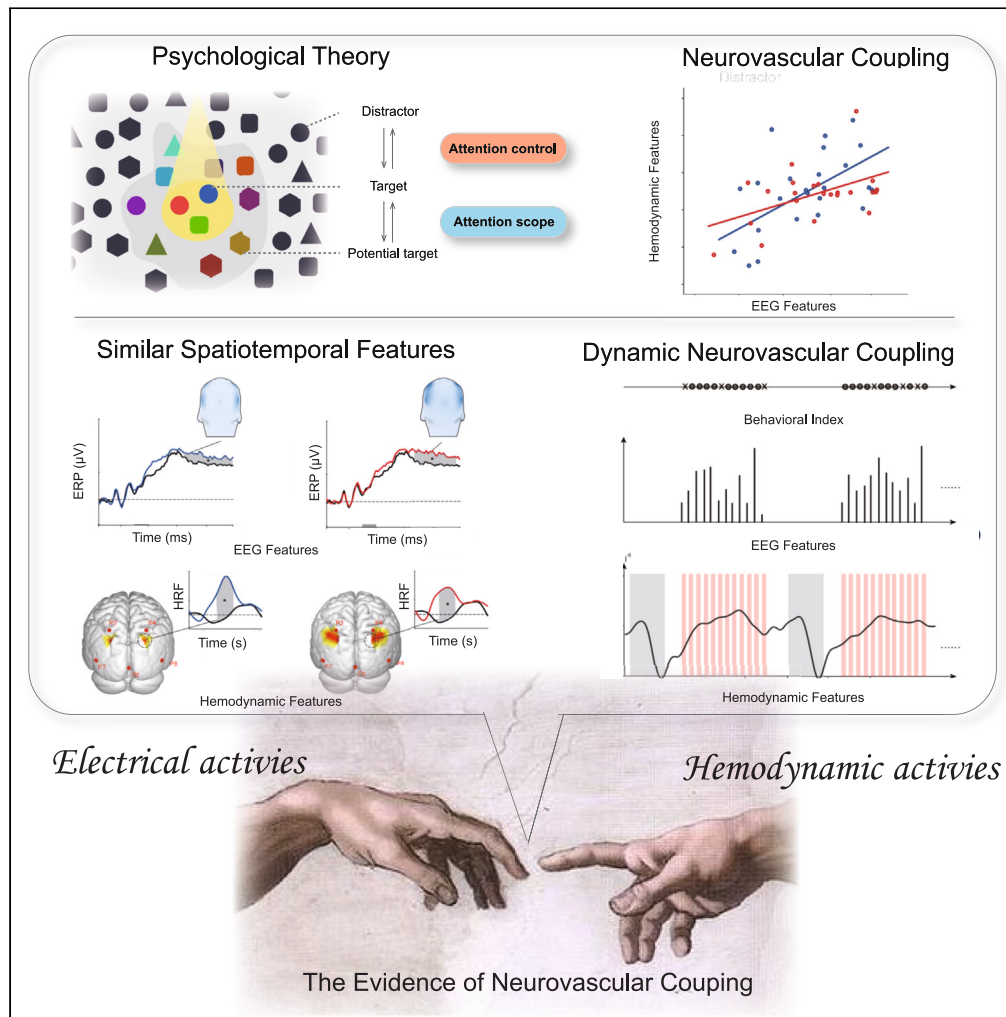


Article

Neurovascular coupling in the attention during visual working memory processes



Hao Zhang, Yiqing Hu, Yang Li, ..., Xiaoli Li, Yan Song, Chenguang Zhao

chenguang918.zhao@gmail.com

Highlights

Multimodal data reveals common NVC in vWM

NVC mechanisms differentiate attention control and scope in vWM

The NVC of attention control shows broad engagement in frontoparietal network

Dynamic NVC of attention control features predict behavior better than other metrics



Article

Neurovascular coupling in the attention during visual working memory processes

Hao Zhang,^{1,2,7,8} Yiqing Hu,^{3,8} Yang Li,³ Dongwei Li,^{4,5} Hanli Liu,⁶ Xiaoli Li,^{2,4} Yan Song,⁴ and Chenguang Zhao^{1,2,3,9,*}

SUMMARY

Focusing attention in visual working memory (vWM) depends on the ability to filter distractors and expand the scope of targets. Although many properties of attention processes in vWM have been well documented, it remains unclear how the mechanisms of neurovascular coupling (NVC) function during attention processes in vWM. Here, we show simultaneous multimodal data that reveal the similar temporal and spatial features of attention processes during vWM. These similarities lead to common NVC outcomes across individuals. When filtering out distractors, the electroencephalography (EEG)-informed NVC displayed broader engagement across the frontoparietal network. A negative correlation may exist between behavioral metrics and EEG-informed NVC strength related to attention control. On a dynamic basis, NVC features exhibited higher discriminatory power in predicting behavior than other features alone. These results underscore how multimodal approaches can advance our understanding of the role of attention in vWM, and how NVC fluctuations are associated with actual behavior.

INTRODUCTION

In daily life, continuous visual information is maintained and manipulated over short intervals in visual working memory (vWM) to guide ongoing behavior.¹ We encode, maintain, and retrieve using our vWM, which largely represents the involvement of attention.² A limited number of available vWM “slots”^{3,4} or limited resource allocation⁵ requires attention processes that govern access to the mnemonic processes.⁶ Various attention processes that dynamically interact with vWM have been studied, including vigilance,⁷ selective attention,⁸ and sustained attention.⁹

Prior work has shown that individuals with higher vWM capacity demonstrate higher attention performance.¹⁰ At the within-subjects level, attention and vWM covary on a moment-to-moment basis and lapse together.¹¹ Extensive theoretical work on information processing has long been conducted on the role of attention in vWM.^{12,13} According to independent contributions to vWM performance, attention processes can be subcategorized into scope and control, which have gradually become different basic conceptualizations of attention in vWM.^{14,15} The scope of attention is an important aspect that is theoretically and empirically related to the storage of vWM, and its changes affect the number of items that can be maintained in vWM.¹² In addition, an individual’s ability to efficiently filter relevant information from irrelevant information contributes to their vWM capacity.^{12,16} Attention control is essential for filtering out surrounding distractors when individuals need to prioritize to-be-remembered information.^{17,18}

Behavioral studies have demonstrated that the scope and control measures of attention have a significant positive correlation.^{14,15,19} The neural explanation is that the two attention processes in vWM have one putative source in the frontoparietal network (FPN), which is related to the bias and maintenance of goal-relevant information within certain scopes.²⁰ The scope and control of attention may have interrelated spatial-temporal characteristics that have been well documented using electroencephalography (EEG), functional near-infrared spectroscopy (fNIRS), and functional magnetic resonance imaging (fMRI). More specifically, the strength of the hemodynamic response²¹ and the amplitude of EEG contralateral delay activity (CDA)^{22–24} in the posterior parietal cortex (PPC) can be used to track the number of items maintained in vWM. Several EEG studies have shown that theta oscillations in the prefrontal cortex (PFC) are typically associated with the scope of vWM, as well as attention control.^{25,26} The prefrontal areas show increased blood-oxygen-level-dependent responses to increases in the vWM scope or attention control.²⁷ However, most previous studies have used unimodal recording or parallel analysis methods, making it

¹School of Systems Science, Beijing Normal University, Beijing 100875, China

²Center for Cognition and Neuroergonomics, State Key Laboratory of Cognitive Neuroscience and Learning, Beijing Normal University at Zhuhai, Zhuhai 519087, China

³Chinese Institute for Brain Research, Beijing 102206, China

⁴State Key Laboratory of Cognitive Neuroscience and Learning, Beijing Normal University, Beijing, China

⁵Department of Applied Psychology, School of Arts and Sciences, Beijing Normal University, Zhuhai, China

⁶Department of Bioengineering, the University of Texas at Arlington, Arlington, TX, USA

⁷International Academic Center of Complex Systems, Advanced Institute of Natural Sciences, Beijing Normal University, Zhuhai, China

⁸These authors contributed equally

⁹Lead contact

*Correspondence: chenguang918.zhao@gmail.com

<https://doi.org/10.1016/j.isci.2024.109368>



difficult to provide a more comprehensive insight into the function of attention during vWM. For example, hemodynamic activity only indirectly reflects the underlying patterns of electrical neural activity, mainly because of slow neurovascular interactions,^{28,29} which are known as neurovascular coupling (NVC). Different brain regions or populations have different NVC relationships,³⁰ which have implications for understanding the disrupted NVC that occurs during neuropsychiatric disorders³¹ and aging.³² NVC is related to cognitive function, including perception,³³ motor control,³⁴ and attention.^{35,36} In particular, the NVC of attention has an important influence on behavioral performance owing to its substantial flexibility in polarity and strength variability between individuals.³⁶ However, attention is not constant and varies over time within individuals.³⁷

Therefore, in the current study, we aimed to first identify the NVC mechanism underlying attention control and scope during vWM and then explore the associations between fluctuations in NVC and actual behavior. We chose the prefrontal theta and parietal CDA, two robust vWM biomarkers, as the main temporal features.³⁸ The spatial resolution of fNIRS was leveraged to functionally localize subject-specific regions of interest (ROIs) in the PFC and bilateral PPC. We further proposed a dynamic EEG-informed algorithm to estimate NVC by integrating temporally sensitive EEG information and spatially sensitive fNIRS information.

A vWM paradigm with three conditions²⁴ was used to isolate the attention activity in the vWM that occurs between the presentations of the to-be-remembered array and a subsequent probe display. We tracked the changes in biological and behavioral metrics by varying the number of targets or distractors to isolate distinct control (filtering efficiency) and scope (buffering capacity) activities. More specifically, when compared with the “2 targets” condition (abbreviated as 2T), increasing the set size of the distractor in the “2 targets + 2 distractors” condition (abbreviated as 2T2D) can be attributed to differences in control of attention and not to task difficulty per se,²⁴ and increasing the set size of the target in the “4 targets” condition (abbreviated as 4T) was used to measure attention scope during vWM task.³⁹ These experimental and analytical frameworks have the potential to aid our understanding of the NVC mechanism of attention during vWM.

RESULTS

Behavioral results

To measure the control and scope of attention during the vWM tasks, we used a change-detection paradigm,²⁴ which required participants to remember the orientations of red bars in the cued hemifield (Figure 1A). After a 900 ms delay, participants indicated whether the probe was in the same orientation as initially presented in the cued hemifield. We calculated vWM performance using a standard formula.²⁴ The K value denotes the number of targets maintained in vWM from N to-be-remembered items. For descriptive purposes, between-condition comparisons relative to baseline conditions are named “attention scope” and “attention control” processes, respectively. The results showed a ceiling effect ($K = 1.942 \pm 0.025$ VS. $N = 2$) for the 2T condition. The indices for attention scope were chosen as the maximum K value (2.117 ± 0.488) through comparison between the 4T and 2T conditions. A higher scope value indicated a larger attention scope. The indices for attention control (1.749 ± 0.207) were defined as the difference in K values between the 2T2D condition and 2T condition.^{19,24} A higher attention control value indicated a better ability to filter distractors. Our results showed that the indices for scope were significantly correlated with those for control (Pearson's $r = 0.406$, $p = 0.001$, Figure 1B), highlighting that individuals with larger scopes had better attention control in filtering out distractors. This result is consistent with previous research.¹⁸

Spatiotemporal features in the PFC

Simultaneous EEG and hemodynamic signals were collected and analyzed using a miniblock design paradigm (Figure 1C). As shown in Figure 1D, we measured the concentration changes in oxygenated hemoglobin (ΔHbO) and deoxygenated hemoglobin (ΔHbR) in the PFC and PPC, as well as whole-brain EEG data. It has been reported that frontal theta is a prominent EEG feature in attention or WM tasks, and is theorized to play important roles in either the control or scope of attention representations.^{14,15} We estimated this modulation of frontal theta power during the retention of vWM by calculating theta event-related synchronization (ERS). Consistent with previous studies,^{25,40} the amplitudes of theta ERS in the three conditions increased by approximately 100–400 ms after memory onset (Figure 2A; false discovery rate [FDR] $p < 0.050$, two-tailed), suggesting that theta power served as a possible carrier frequency for vWM processes.⁴¹ To further segregate control-related and scope-related theta activities, we compared the baseline conditions (2T) with the other two conditions. As shown in Figure 2A, theta ERS significantly increased in the 2T2D condition (from 120 to 390 ms) and 4T condition (from 140 to 400 ms) relative to the 2T condition (cluster-based permutation test: $p < 0.050$, two-tailed). The differences shown in the topographic maps were averaged over the significant time points. The scalp distributions of increasing theta ERS in both the 2T2D and 4T conditions were mostly expressed over the same prefrontal electrodes (F3, FZ, and F4). No significant difference in theta ERS was found between the 2T2D and 4T groups ($p > 0.371$; $\text{BF}_{10} = 0.101$). Our EEG results showed similar scalp distributions and time course profiles for control and scope of attention in vWM.

We then focused on the difference in hemodynamic activity (as indicated by ΔHbO levels) related to the scope and control of attention. For attention control, paired t tests showed that significant increases in hemodynamic responses were found in the PFC near the F4 electrode and defined the control ROI (Figure 2B; channels 36 and 32; FDR $p < 0.050$, two-tailed). We also found a significant increase in the ΔHbO response for attention scope in the partially overlapping regions of the control and defined scope ROI (Figure 2B; channels 36 and 31; FDR $p < 0.050$, two-tailed). Structural MR images with extra anatomical landmarks (vitamin E capsules) were used to project the fNIRS channels onto the cortical surface using the near-infrared spectroscopy statistical parametric mapping (NIRS-SPM) package⁴² and to determine the anatomical localization of each fNIRS measurement channel. The results showed that the anatomical localization of the scope and control ROI was in the frontal eye field (FEF) (Table S1). The overlapping channels (channel 36) were used to show the time course of the memory response using

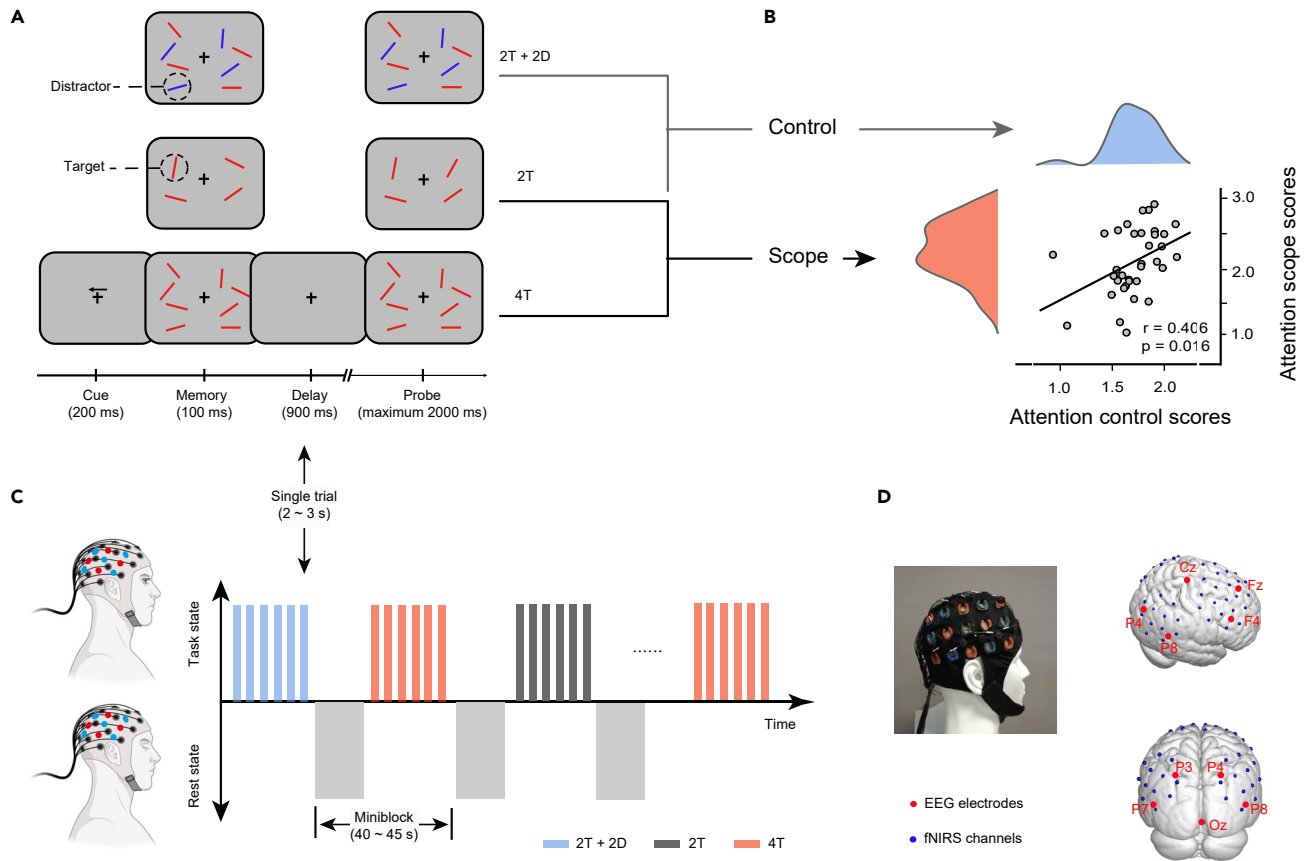


Figure 1. Experimental design and simultaneous data acquisition

(A) vWM task: two targets (2T), two targets and two distractors (2T+2D), and four targets (4T); these three conditions were designed to isolate the control and scope of attention during vWM by comparing to baseline conditions (2T).

(B) Correlation of control and scope: a robust positive relationship between attention control (blue, bottom axis) and attention scope (red, right axis).

(C) Miniblock design nesting rest state: by introducing a closed-eye period between miniblocks, a transition between task and rest states is achieved while preventing temporal overlap of prior hemodynamic responses.

(D) Sensor localization: a photograph of the sensor cap and side/rear views of EEG electrodes (red) and fNIRS channels (blue), covering regions of interest, such as the prefrontal cortex and posterior parietal cortex.

general linear model (GLM) analysis.⁴³ The attention scope led to a significant increase of ΔHbO from 4.1 s to 7.6 s locked to memory display (cluster-based permutation test: $p < 0.050$, Figure 2B). Similar to attention scope, a significant increase of ΔHbO from 3.8 s to 7.7 s was observed for the attention control. No significant difference in ΔHbO was found between the 2T2D and 4T groups ($p > 0.241$; $\text{BF}_{10} < 0.207$).

We performed between-subject correlation analyses to quantify the NVC between theta ERS and ΔHbO activation. As shown in Figure 2C, the difference in theta ERS between the corresponding condition and baseline was positively correlated with hemodynamic differences within the functional ROIs (attention control: $r = 0.508$, $p < 0.011$; attention scope: $r = 0.457$, $p = 0.028$, two-tailed). As mentioned previously (Figure 2), both theta ERS and ΔHbO activations have similar spatiotemporal characteristics in the PFC and NVC between the individual levels, which suggests that scope and control processes might share common functional mechanisms in the PFC.

Spatiotemporal features in the PPC

We used CDA as an EEG marker for the vWM in humans to track changes in active storage during vWM retention of vWM.²³ Consistent with many previous studies,^{22–24} our results showed that a sustained negative potential with a posterior scalp distribution persisted during the delay period (Figure 3A; $\text{FDR } p < 0.050$, two-tailed). EEG CDA amplitudes were compared across the conditions to assess the scope and control of attention. As shown in Figure 3A, the amplitude of EEG CDA increased from 425 to 900 ms as the attention scope increased (Figure 3A; cluster-based permutation test: $p < 0.050$, two-tailed), which is consistent with the fact that the posterior CDA amplitude was sensitive to the mnemonic load.⁴⁴ For attention control, our results showed that the CDA amplitude significantly increased from 477 to 900 ms (cluster-based permutation test: $p < 0.050$, two-tailed). The topographic maps of these differences over the significant time points showed similar scalp distributions, where they were mostly expressed over the same posterior parietal electrodes: P3 (paired P4) and P7 (paired P8). No significant

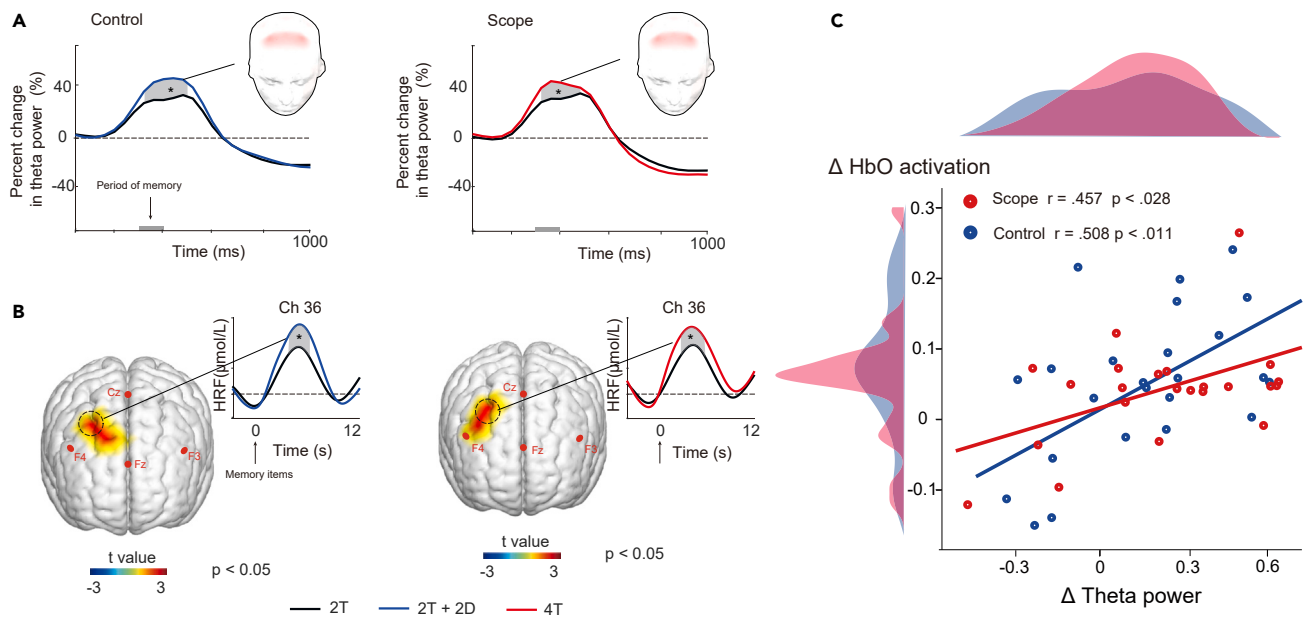


Figure 2. Spatiotemporal features in the PFC

(A) Frontal theta ERS: a consistent increase at approximately 120–400 ms post memory onset; the red-shaded region indicates significant electrodes (frontal view). The gray-shaded regions, marked with asterisks, indicate statistically significant time intervals.

(B) Hemodynamic activation: the brain map highlights changes in Δ HbO responses within brain regions exhibiting statistically significant t values (frontal view) compared to the baseline condition. The Δ HbO signal response exhibits a similar temporal pattern.

(C) NVC analysis across subjects: the correlation between relative changes in Δ theta power and Δ HbO within ROIs demonstrate a positive correlation, with the shaded areas on the left and top axes indicating the distribution of values for each feature. * $p < 0.05$.

difference in the EEG CDA was found between the 2T2D and 4T conditions ($p = 0.114$; $BF_{10} = 0.217$). Our EEG results showed that the control and scope of attention were involved in CDA changes, with similar scalp distributions and time course profiles.

To investigate the metabolic features related to attention in the vWM, we quantified hemodynamic CDA using an approach similar to EEG analysis for each pair of symmetrical PPC channels.

We multiplied the beta values by using basis functions to obtain the hemodynamic response function (HRF) time-domain waveforms. We then used a cluster-based permutation test to identify the latency of the hemodynamic CDA. The results (Figure S1) showed that the significant hemodynamic CDA (contralateral > ipsilateral responses) in the 2T2D (from 1.8 to 5.5 s) and 4T conditions (from 1.1 to 5.4 s). We further calculated the mean Δ HbO within 2–5s after stimulus onset for each trial, and performed statistical tests on the ipsilateral and contralateral responses. For 4T condition, the memory-related increases were found in contralateral HRF ($p < 0.02$, two-tailed), but not in ipsilateral HRFs ($p > 0.411$; $BF_{10} = 0.125$) when compared with 2T condition. These results suggest that a significant hemodynamic CDA effect was measured using fNIRS. We additionally conducted a correlation analysis between contralateral increases in HRFs (from 2T to 4T condition) and behavioral K values across the subjects. We found a significant positive correlation ($r = 0.451$, $p < 0.04$, two-tailed). This suggests that the greater the amplitude of contralateral HRF, the higher the K value. This result is consistent with previous findings that activity in the PPC is tightly correlated with the limited amount of information that can be stored in working memory.²¹

For attention control, paired t tests showed that significant hemodynamic CDA increases were found in the PPC near the region between the P3 and P7 electrodes (channels 10 and 9 in Figure 2B; $FDR p < 0.050$, two-tailed). We also found a significant increase in hemodynamic CDA for attention control in the overlapping (channels 10 and 20) and extra regions (channels 9 and 21), as shown in Figure 3B ($FDR p < 0.050$, two-tailed). The results (Table S2) showed that the anatomical localization of bilateral channels 10 (paired 20) and 9 (paired 21) projected into the bilateral superior parietal lobe (SPL). The waveform of hemodynamic CDA in the overlapping channels (channel 10) showed that the memory item led to a significant increase of hemodynamic CDA from 2.4 s to 7.1 s for the attention scope (cluster-based permutation test: $p < 0.050$, Figure 3B). Similarly, a significant increase from 2.0 s to 6.6 s was observed for the attention control. No significant difference in Δ HbO was found between the 2T2D and 4T groups ($p > 0.211$; $BF_{10} < 0.307$).

As illustrated in Figure 3C, the difference in hemodynamic CDA activation was closely and positively correlated with the difference in EEG CDA amplitude across all participants (attention control: $r = 0.446$, $p < 0.040$; attention scope: $r = 0.563$, $p < 0.020$), suggesting that the greater the increase in posterior CDA amplitudes, the greater the increase in local hemodynamic CDA observed near the corresponding electrodes. Note that the EEG CDA amplitudes were negative, and the y axis in Figure 3A is plotted as negative-up. To render its polarity consistent relative to the trend of CDA, we show the negative-right axis of Δ CDA in the correlation scatterplot. In addition, we analyzed the parietal contralateral alpha power suppression (8–12 Hz), which was also observed during the vWM tasks. No significant differences were found among the

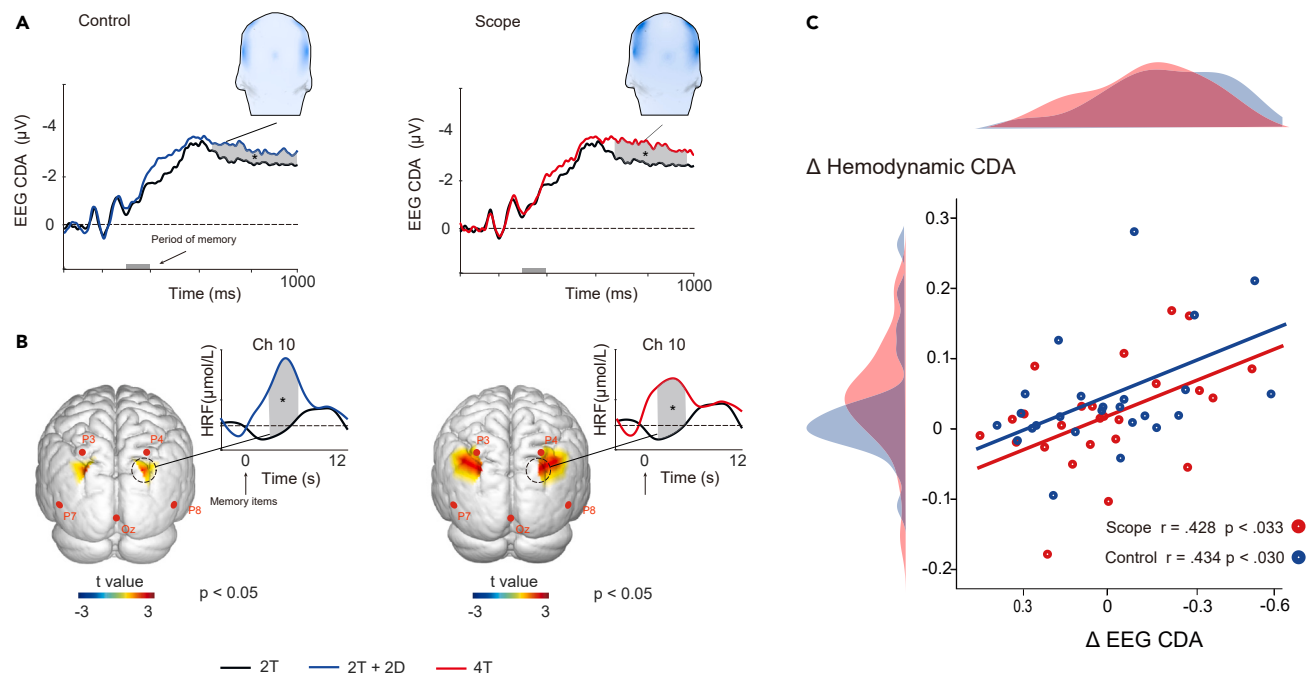


Figure 3. Spatiotemporal features in the PPC

(A) EEG CDA: variation during the delay period revealed sustained negative potential changes (amplitude axis reversed), with the blue-shaded region indicating significant electrodes (posterior view). The gray-shaded regions, marked with asterisks, indicated statistically significant time intervals.

(B) Hemodynamic CDA: the brain map highlights changes in contralateral effects within brain regions exhibiting statistically significant t values (posterior view) compared to the baseline condition. The ΔHbO signal response exhibits a similar temporal pattern.

(C) NVC analysis across subjects: the extracted characteristics from $\Delta\text{EEG CDA}$ and Δ hemodynamic CDA demonstrate a positive correlation for attention control and scope, with the shaded areas on the left and top axes indicating the distribution of values for each feature. * $p < 0.05$.

three conditions ($p > 0.577$). We also analyzed the ΔHbR concentration by using the same methods as those used for the ΔHbO data. Neither a significant activation nor a reliable correlation between the ΔHbR concentration and corresponding EEG features was found for any condition.

EEG-informed NVC

Thus far, we have outlined the basic NVC for the scope and control of attention at between-subject levels. EEG activities (CDA or theta power) seem to be accompanied by resulting metabolic variation. This qualitative NVC analysis was conducted under the simplifying assumption that the NVC was constant for every individual throughout the experiment. We further explored the NVC mechanisms underlying the control and scope of attention using EEG-informed NVC analysis, which can move beyond the above correlational analyses by monitoring and assessing the trial-by-trial variance in inter-subject activity. We hypothesized that posterior CDA and frontal theta ERS have links with the ΔHbO concentration variation at within-subject levels, resulting in observed significant EEG-informed NVC. To quantify NVC, EEG-informed NVC analysis modeled the association between hemodynamic activity and WM-derived EEG characteristics using a GLM, and t-contracts showed the significance of the coefficients related to the WM-derived EEG regressors in the GLM at the within-subject level. In the 2T2D condition, frontal theta ERS was positively correlated with ΔHbO in the right FEF and right SPL (Figure 4A, first row, $\text{FDR } p < 0.05$). That is, front theta ERS was more elevated when these brain regions were more active on a trial-by-trial basis. The bilateral SPL and FEF showed significant NVC with posterior CDA amplitudes (Figure 4A, second row, $\text{FDR } p < 0.05$, two-tailed). For the 4T condition, regions showing significant NVC in the frontal theta ERS included only the FEF and not the SPL (Figure 4B, first row, $\text{FDR } p < 0.05$, two-tailed). The coordinates of the regions showing significant NVC are listed in Table S3. For EEG CDA from the PPC, areas showing positive NVC included regions within the right SPL (Figure 4B, second row, $\text{FDR } p < 0.05$, two-tailed). That is, on a trial-by-trial basis, these brain regions showed increased ΔHbO activity when the CDA amplitude increased. As expected, increased use of posterior CDA or frontal theta power were both accompanied by the increased adjacent ΔHbO for the 2T2D and 4T conditions. Interestingly, our results showed that the NVC in 2T2D is involved in a broad range of brain regions, some of which are part of the FPN. In contrast, no significant NVC was observed across regions in the 4T condition ($p > 0.358$). This difference in the activated regions of the NVC led to dissociation of the mechanisms of scope and control of attention during vWM, suggesting that NVC can be characterized by substantial flexibility in its polarity and spatiotemporal variability.⁴⁵

Further, we tracked the changes in NVC strength by comparing them with the 2T condition to isolate distinct control and scope activities. Statistical analysis was performed using a paired t test to define the significant brain regions where the trial-by-trial coupling effect was significantly greater than in the 2T condition. For attention control, paired t tests showed significant theta-informed NVC increases in the right SPL

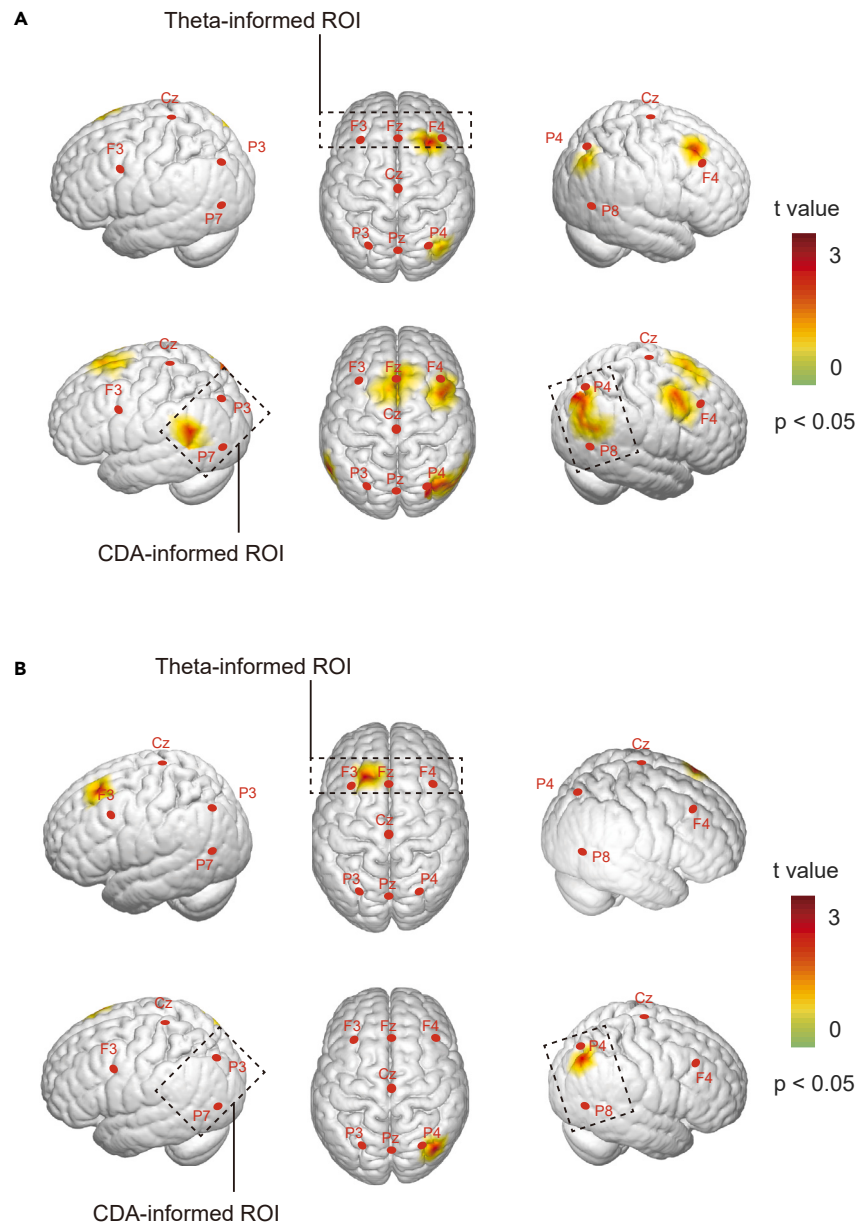


Figure 4. The EEG-informed NVC strength in two conditions

(A) EEG-informed NVC for attention control. The t map shows the significant theta-informed NVC (upper panel) in the middle frontal gyrus and SPL and CDA-informed NVC (bottom panel) in the bilateral SPL and middle frontal gyrus.

(B) EEG-informed NVC for attention scope. The t map shows the significant theta-informed NVC (upper panel) in the middle frontal gyrus, and CDA-informed NVC (bottom panel) in the bilateral SPL.

(first row in Figure S2; FDR $p < 0.050$, two-tailed). The coordinates of the regions showing significant NVC are listed in Table S4. In addition, we found a significant increase in the CDA-informed NVC for attention control in the overlapping (bilateral SPL and medial frontal gyrus [MFG]) and extra regions (channels 9 and 21), as shown in the second row (FDR $p < 0.050$, two-tailed). In contrast, no significant difference in NVC between 4T and 2T was observed for attention scope ($p > 0.358$). This difference in NVC dissociates the mechanisms of scope and control of attention during vWM.

Dynamic NVC and K value

First, we transferred the analytical framework to a novel dynamic behavioral performance and NVC built on miniblock experimental designs. Moreover, we conducted a modeling analysis of how dynamic NVC can influence dynamic behavior, as measured by the K value. In the frontal

theta-informed NVC, the FEF showed a significant cluster in the 2T2D condition. No significant clusters were found in the other conditions or EEG-informed NVC ($p > 0.217$; $BF_{10} < 0.301$). The negative coefficient indicated that the frontal theta ERS was more closely coupled to adjacent ΔHbO signals, as was the smaller dynamic K value.

We also performed a correlation analysis between dynamic NVC and dynamic K values. Results showed that the K values were smaller in miniblocks with a weaker NVC of theta ERS across subjects (Spearman's $r = -0.113$, $p = 0.014$, two-tailed). We further calculated the average miniblock NVC for each quartile to confirm the relationship between the frontal theta NVC and the K value. Repeated-measures analysis of variance (ANOVA) of NVC showed that normalized NVC decreased with an increase in the K value in the 2T2D condition ($F_{3, 75} = 4.450$, $p = 0.007$). The results in Figure 5C show that the NVC in the fourth quartile was significantly smaller than that in the first ($t = 3.599$, $p = 0.002$, Cohen's $d = 0.750$) and third quartiles ($t = 2.851$, $p = 0.009$, Cohen's $d = 0.594$). Similarly, no significant differences were found among the quartiles ($p > 0.239$) for the other conditions.

Receiver operating characteristic (ROC) analysis was used to compare the sensitivity and specificity of various WM-related metrics for predicting the dynamic performance in the 2T2D condition. We evaluated the performance of the GLM analysis concerning EEG, ΔHbO , and NVC metrics (Figure 5D). One-way repeated measures ANOVA indicated a significant effect of the model type ($F_{2,44} = 3.339$, $p = 0.045$) on the area under the curve (AUC) values that represented the sensitivity and specificity of the model. The posthoc test indicated that the NVC-based model achieved the highest AUC, and it was significantly higher than the EEG-based ($t = 1.929$, $p = 0.033$, Cohen's $d = 0.402$) and ΔHbO ($t = 2.330$, $p = 0.015$, Cohen's $d = 0.486$) model. Finally, when fitting the model to predict the performance of attention scope, no significant difference in AUC was found among the three WM-related metrics ($p > 0.271$). These results indicate that NVC for the control of attention can be predictive of behavioral outcomes and, therefore, is likely to play an important role in cognitive processes related to memory and attention. We also analyzed the data based on reaction times and variance in reaction times using the same methods, but no significant results were found for any of the conditions ($p > 0.427$).

DISCUSSION

In this study, we investigated spatiotemporal features and the corresponding NVC for attention scope and control during vWM using both temporally sensitive EEG markers and spatially sensitive hemodynamic activation. The main findings were as follows. (1) The multimodal results showed that the control and scope processes in vWM evoked similar temporal profiles of frontal theta ERS or posterior CDA, and similar distributions of hemodynamic activation within the FEF and SPL. We provide crucial converging evidence that the control and scope processes share a similar NVC mechanism at both the trial and trait levels, except that attention control involves a broad range of NVC within the FPN. (2) The fluctuations of theta-informed NVC within SPL can be predictive of the performance to filter out distractors. There may be a negative relationship between behavioral metrics and dynamic NVC strengths. Moreover, theta-informed NVC may be a potential candidate for predicting behavioral performance involving attention control. In summary, these results highlight the fact that multimodal approaches can advance our understanding of NVC attention mechanisms in vWM.

The NVC and attention research

The first study⁴⁶ utilized simultaneous EEG-fMRI recordings during verbal WM tasks in a long-term trial (>10 s). However, investigations of the attentional aspects of vWM, such as scope and control processes, are rare. This might be because acoustic noise during fMRI scanning requires additional attention resources, which are confounding factors during an attention task.⁴⁷ The use of EEG-fNIRS has paved the way for ecologically valid settings to eliminate acoustic artifacts from fMRI scans. Some EEG-fNIRS studies have focused on verbal WM⁴⁸ or vWM using parallel analysis.⁴⁹ Few studies have investigated attention during vWM. The main reason for this is the lower certainty and greater complexity of attention tasks compared to simple sensory and motor tasks.⁵⁰ To exclude potential confounding effects, such as motivation, strategies, and adaptive habits, two of the three conditions were combined to isolate distinct attention-related processes. Another challenge in effectively measuring the NVC mechanism is the mismatched timescales between EEG and hemodynamic signals. The most popular task design among EEG-fNIRS studies is the block design, which improves the accommodation of block designs for a relatively slow hemodynamic response compared with event-related designs. However, block designs also resulted in a higher susceptibility to anticipation and habituation effects, which should be avoided in rapid event-related EEG studies.⁵¹ Moreover, if the experiment duration is limited and intertrial intervals (ITIs) persist for longer than 10 s, the number of trial repetitions per condition decreases, potentially lowering the EEG signal-to-noise ratio (SNR). To address this dilemma, we used a mixed block/event-related fMRI design that allowed for a fuller characterization of time-sensitive and nonlinear activities.⁵² The active eye-closed resting state could accelerate the return of the hemodynamic signal to baseline to ensure that hemodynamic variations are not artifacts caused by the prior signal. This miniblock design of a nested resting state is thought to balance the trade-offs between minimized crossover effects from inherently slow hemodynamic signals, and pursues a higher signal-to-noise ratio from a greater EEG response.

NVC with frontal theta activities

Frontal theta oscillations play a causal role in facilitating increases in vWM capacity, which are thought to be linked to frontal theta power²⁵ or theta synchronizations.⁵³ Our oscillatory results showed that there was a greater increase in the frontal theta power as target or distractor items increased. This is consistent with the idea that increased frontal theta power during the period of vWM representation plays a positive

On a trial-by-trial basis, when distractors were filtered out, frontal theta ERS was more elevated when the brain regions in the right FEF and right SPL were more active. In contrast, when there were no distractors but rather extra targets, the NVC of the frontal theta ERS included only the FEF. A possible explanation for this might be that attention control is associated with widespread NVC. To the best of our knowledge, theta-band oscillations have been proposed as carrier frequencies for attention control.⁵⁷ In this case, we suggest that the hemodynamic activity of these two regions could be coupled with frontal theta activity.

NVC with posterior CDA

The CDA amplitudes within the PPC increased during the retention period (approximately 400–1,000 ms) when the set size of the distractors or the scope of the targets increased. This finding is consistent with previous studies that used changes in CDA amplitude to track and compare the number of items maintained in vWM.²³ From the synchronously observed fNIRS results (Figure 3), hemodynamic CDA originated from the contralateral effect in the PPC to the visual field of the target, which was reported in previous fNIRS studies using the lateralized event-related potential (ERP) approach.^{35,36} The rise in hemodynamic CDA in the bilateral SPL as the scope of the target in vWM increased from two to four items is in agreement with previous studies.^{21,39}

In this study, we developed synchronous measurements and analyses of multimodal contralateral delay activities and, for the first time, calculated the relationship between electrical and hemodynamic CDA. Our results showed that changes in hemodynamic CDA were positively correlated with changes in EEG CDA amplitude in the PPC during active maintenance. Given that the set-size effects of EEG CDA are accepted neurophysiological measures for the range of items held in vWM,⁵⁸ when the scope of targets increases, hemodynamic CDA is likely to reflect the linearly related metabolic demands supporting simultaneous EEG CDA during a certain period. In this sense, the role of increased hemodynamic CDA in attention control might stem from the increased demand for oxygen, as distractors that failed to filter were maintained in the vWM. In similar fMRI/fNIRS studies,^{39,59–61} lateralized effects of delay period activity were found in brain regions such as the occipital lobe, superior temporal sulcus, and intraparietal sulcus (IPS–IOS). These effects have a potential association with task load. However, the observation of activation in the hemodynamic CDA component may seem novel in the context of fNIRS research. Possible reasons for this are as follows. (1) The fNIRS signals are susceptible to factors such as scalp blood flow variations, heart rate, and respiration. The increased sample size (more participants and more trials) may result in greater strength and statistical power for our study. (2) The miniblock design might be the element enabling its successful detection. The miniblock design with short inter-stimulus intervals employed in our study likely amplified the lateralized effects compared to trial or block designs. (3) The interspersed closed-eye resting periods not only promoted rapid resetting of oxygen metabolism, but also ensured the maintenance of relatively consistent hemodynamic responses throughout the task, thereby addressing a critical limitation encountered in prior investigations. Further studies are needed to verify whether the implementation of miniblock design and utilization of closed-eye resting constitute pivotal factors facilitating the successful detection of the hemodynamic equivalent of CDA using fNIRS technology.

In addition, the bilateral SPL and MFG showed significant CDA-informed NVC for attention control but not MFG for attention scope. Our results suggest that these areas are specifically involved in filtering out simultaneous distractors, which is consistent with previous research findings demonstrating that spatial filtering leads to increased activity in posterior regions, including the middle temporal gyrus and middle occipital gyrus.⁶² Given that the posterior CDA amplitude can be used to track the number of distractors inadvertently reaching the vWM, it is plausible that EEG CDA may be linked to hemodynamic activity in the frontal and parietal regions. This represents a likely mechanism of vWM processes, in which the PFC is engaged in attention control to filter out distractors existing in the PPC buffer for vWM.

The relationship between NVC and behavior

Recent studies have made considerable headway in understanding how attention guides behavior in this dynamic manner when completing an entire cognitive task.⁶³ The capacity to stabilize the content of attention not only varies across individuals, but is also time-varying within individuals.⁶⁴ This means that attention during the vWM task is not static, nor is it possible or desirable for each miniblock to simultaneously label the unique NVC calculated at the group level. Rather, failures to filter distractors are frequent and the scope of attention fluctuates, paced by the natural speed of the attention systems that govern access to vWM. The relationship between task-related NVC strength and behavior performance has been assessed across individuals,⁶⁵ with subject-level analyses not reported. To fill this knowledge gap, we first continuously tracked the fluctuations in vWM processing at various levels of psychophysiological reactions (see Figure 5), and then for each miniblock, quantized the dynamic NVC between moment-to-moment changes in brain activity and continuous readouts of behavior. The results of modeling (explained behavioral data) showed that the dynamic NVC of frontal theta activity within the FEF has a robust negative relationship with K values for attention control processes. Huo et al. reported neurovascular decoupling where the firing rate and oscillatory power in the frontal cortex of head-fixed mice increased as hemodynamic activity did not change during locomotion.⁶⁶ We suggest that NVC strength between frontal theta activities and Δ HbO plays an important role in controlling distractors filtered out of vWM. More specifically, the decoupling or coupling of neural activity from hemodynamic signals might determine whether attention control is zoomed in or out in vWM. This relationship should be interpreted with caution, unless detailed NVC mechanisms linking attention control are available at the microscopic and mesoscopic levels.⁶⁷ In addition, diagnostic accuracy evaluation demonstrated that NVC had higher discriminatory power for predicting behavior than EEG features and fNIRS features alone, which is consistent with the idea of enhanced classification and decoding accuracy over a single modality in various tasks for brain-computer interfaces.⁶⁸

Limitations of the study

There are some limitations in the current study. First, although we provided converging evidence for NVC analysis at both the between- and within-subject levels, individual difference correlations based on relatively modest sample sizes make it challenging to build robust correlations across individuals due to possible inflated effect sizes.⁶⁹ Second, a particularly significant disadvantage of EEG-fNIRS when evaluating NVC is that it is limited to superficial neocortical levels. Hence, NVC in deep-seated structures, such as the hippocampus or thalamus, cannot be addressed. Finally, in the change-detection design, the target and distractor lend themselves to the probe array. A model-driven approach, such as lateralized activity analysis and contrast with the baseline condition, was applied to separate attention scope from the memory load. However, the observed hemodynamic or EEG results may have been inflated by WM maintenance processes, rather than reflecting only selection processes in vWM. For example, hemodynamic CDA may be manifestations of distinct processes underlying vWM. It is difficult to attribute all effects to the selection processes and not to implicate further WM maintenance processes. Thus, the scope effects should be interpreted with caution.

Despite these limitations, our study provides novel insights into the NVC mechanisms underlying the scope and control of attention. For future clinical research, the detailed NVC mechanisms underlying basic cognitive processes will be an important step forward in the successful application of relevant theories and methods to measure cognitive deficits associated with a wide variety of neuropsychiatric disorders.^{28,31,67} Our work not only provides a more comprehensive insight into functional activity, but also provides a new perspective for the evaluation and prediction of behavioral performance on a dynamic basis. Individual moment-to-moment differences in filtered-out distractors may be related to fluctuations in theta-informed NVC within the FEF. This provides a promising approach for optimizing spatiotemporal resolution in the closed-loop system of cognitive brain-machine interfaces.

STAR★METHODS

Detailed methods are provided in the online version of this paper and include the following:

- KEY RESOURCES TABLE
- RESOURCE AVAILABILITY
 - Lead contact
 - Materials availability
 - Data and code availability
- EXPERIMENTAL MODEL AND STUDY PARTICIPANT DETAILS
- METHOD DETAILS
 - Working memory task
 - Miniblock nesting rest state design
 - Resting period effectiveness
 - Simultaneous data acquisition
 - Preprocessing
 - Behavior analysis
 - ERP analysis
 - EEG oscillation
 - General linear model
 - Task-related activation
 - Hemodynamic contralateral delay activity
 - EEG-informed analysis
 - Modeling analysis
- QUANTIFICATION AND STATISTICAL ANALYSIS
- ADDITIONAL RESOURCES

SUPPLEMENTAL INFORMATION

Supplemental information can be found online at <https://doi.org/10.1016/j.isci.2024.109368>.

ACKNOWLEDGMENTS

We thank all of the participants who participated in the study.

Funding: The present research was supported by: STI2030 Major Projects (no. 2022ZD0211300 and no. 2021ZD0204300) and National Natural Science Foundation of China (no. 62201064).

AUTHOR CONTRIBUTIONS

Conceptualization, Y.H. and C.Z.; methodology, H.Z. and C.Z.; investigation, Y.H. and Y.L.; visualization, Y.L. and D.L.; supervision, D.L. and H.L.; writing – original draft, H.Z. and C.Z.; writing – review & editing, H.Z., X.L., Y.S., and C.Z.

DECLARATION OF INTERESTS

Authors declare that they have no competing interests.

Received: November 6, 2023

Revised: November 19, 2023

Accepted: February 26, 2024

Published: February 29, 2024

REFERENCES

1. Baddeley, A. (2000). The episodic buffer: a new component of working memory? *Trends Cogn. Sci.* 4, 417–423. [https://doi.org/10.1016/s1364-6613\(00\)01538-2](https://doi.org/10.1016/s1364-6613(00)01538-2).
2. Chun, M.M., and Johnson, M.K. (2011). Memory: Enduring Traces of Perceptual and Reflective Attention. *Neuron* 72, 520–535. <https://doi.org/10.1016/j.neuron.2011.10.026>.
3. Alvarez, G.A., and Cavanagh, P. (2004). The capacity of visual short-term memory is set both by visual information load and by number of objects. *Psychol. Sci.* 15, 106–111. <https://doi.org/10.1111/j.0963-7214.2004.01502006.x>.
4. Barton, B., Ester, E.F., and Awh, E. (2009). Discrete Resource Allocation in Visual Working Memory. *J. Exp. Psychol. Hum. Percept. Perform.* 35, 1359–1367. <https://doi.org/10.1037/a0015792>.
5. Bays, P.M., and Husain, M. (2008). Dynamic shifts of limited working memory resources in human vision. *Science* 321, 851–854. <https://doi.org/10.1126/science.1158023>.
6. Tay, D., and McDonald, J.J. (2022). Attentional enhancement predicts individual differences in visual working memory under go/no-go search conditions. *PLoS Biol.* 20, e3001917. <https://doi.org/10.1371/journal.pbio.3001917>.
7. Helton, W.S., and Russell, P.N. (2011). Working memory load and the vigilance decrement. *Exp. Brain Res.* 212, 429–437. <https://doi.org/10.1007/s00221-011-2749-1>.
8. Downing, P.E. (2000). Interactions between visual working memory and selective attention. *Psychol. Sci.* 11, 467–473.
9. Unsworth, N., and Robison, M.K. (2020). Working Memory Capacity and Sustained Attention: A Cognitive-Energetic Perspective. *J. Exp. Psychol. Learn. Mem. Cogn.* 46, 77–103. <https://doi.org/10.1037/xlm0000712>.
10. Shipstead, Z., Harrison, T.L., and Engle, R.W. (2015). Working memory capacity and the scope and control of attention. *Atten. Percept. Psychophys.* 77, 1863–1880. <https://doi.org/10.3758/s13414-015-0899-0>.
11. DeBettencourt, M.T., Keene, P.A., Awh, E., and Vogel, E.K. (2019). Real-time triggering reveals concurrent lapses of attention and working memory. *Nat. Hum. Behav.* 3, 808–816. <https://doi.org/10.1038/s41562-019-0606-6>.
12. Cowan, N., Elliott, E.M., Scott Saults, J., Morey, C.C., Mattox, S., Hismjatullina, A., and Conway, A.R.A. (2005). On the capacity of attention: Its estimation and its role in working memory and cognitive aptitudes. *Cogn. Psychol.* 51, 42–100. <https://doi.org/10.1016/j.cogpsych.2004.12.001>.
13. D'Esposito, M., and Postle, B.R. (2015). The Cognitive Neuroscience of Working Memory. *Ann. Rev. Psychol.* 115–142. <https://doi.org/10.1146/annurev-psych-010814-015031>.
14. Shipstead, Z., Redick, T.S., Hicks, K.L., and Engle, R.W. (2012). The scope and control of attention as separate aspects of working memory. *Memory* 20, 608–628. <https://doi.org/10.1080/09658211.2012.691519>.
15. Chow, M., and Conway, A.R.A. (2015). The scope and control of attention: Sources of variance in working memory capacity. *Mem. Cognit.* 43, 325–339. <https://doi.org/10.3758/s13421-014-0496-9>.
16. Fukuda, K., and Vogel, E.K. (2009). Human Variation in Overriding Attentional Capture. *J. Neurosci.* 29, 8726–8733. <https://doi.org/10.1523/jneurosci.2145-09.2009>.
17. Kane, M.J., Bleckley, M.K., Conway, A.R., and Engle, R.W. (2001). A controlled-attention view of working-memory capacity. *J. Exp. Psychol. Gen.* 130, 169–183. <https://doi.org/10.1037/0096-3445.130.2.169>.
18. Cowan, N., and Morey, C.C. (2006). Visual working memory depends on attentional filtering. *Trends Cogn. Sci.* 10, 139–141. <https://doi.org/10.1016/j.tics.2006.02.001>.
19. Li, S., Cai, Y., Liu, J., Li, D., Feng, Z., Chen, C., and Xue, G. (2017). Dissociated roles of the parietal and frontal cortices in the scope and control of attention during visual working memory. *Neuroimage* 149, 210–219. <https://doi.org/10.1016/j.neuroimage.2017.01.061>.
20. Eriksson, J., Vogel, E.K., Lansner, A., Bergström, F., and Nyberg, L. (2015). Neurocognitive Architecture of Working Memory. *Neuron* 88, 33–46. <https://doi.org/10.1016/j.neuron.2015.09.020>.
21. Todd, J.J., and Marois, R. (2004). Capacity limit of visual short-term memory in human posterior parietal cortex. *Nature* 428, 751–754. <https://doi.org/10.1038/nature02466>.
22. McCollough, A.W., Machizawa, M.G., and Vogel, E.K. (2007). Electrophysiological measures of maintaining representations in visual working memory. *Cortex* 43, 77–94. [https://doi.org/10.1016/s0010-9452\(08\)70447-7](https://doi.org/10.1016/s0010-9452(08)70447-7).
23. Vogel, E.K., and Machizawa, M.G. (2004). Neural activity predicts individual differences in visual working memory capacity. *Nature* 428, 748–751. <https://doi.org/10.1038/nature02447>.
24. Vogel, E.K., McCollough, A.W., and Machizawa, M.G. (2005). Neural measures reveal individual differences in controlling access to working memory. *Nature* 438, 500–503. <https://doi.org/10.1038/nature04171>.
25. Riddle, J., Scimeca, J.M., Cellier, D., Dhanani, S., and D'Esposito, M. (2020). Causal Evidence for a Role of Theta and Alpha Oscillations in the Control of Working Memory. *Curr. Biol.* 30, 1748–1754.e4. <https://doi.org/10.1016/j.cub.2020.02.065>.
26. Jones, M.W., and Wilson, M.A. (2005). Theta rhythms coordinate hippocampal-prefrontal interactions in a spatial memory task. *PLoS Biol.* 3, e402–e2199. <https://doi.org/10.1371/journal.pbio.0030402>.
27. Schwartz, S., Vuilleumier, P., Hutton, C., Maravita, A., Dolan, R.J., and Driver, J. (2005). Attentional load and sensory competition in human vision: modulation of fMRI responses by load at fixation during task-irrelevant stimulation in the peripheral visual field. *Cereb. Cortex* 15, 770–786. <https://doi.org/10.1093/cercor/bhh178>.
28. Kaplan, L., Chow, B.W., and Gu, C. (2020). Neuronal regulation of the blood-brain barrier and neurovascular coupling. *Nat. Rev. Neurosci.* 21, 416–432. <https://doi.org/10.1038/s41583-020-0322-2>.
29. Drew, P.J. (2022). Neurovascular coupling: motive unknown. *Trends Neurosci.* 45, 809–819. <https://doi.org/10.1016/j.tins.2022.08.004>.
30. Devonshire, I.M., Papadakis, N.G., Port, M., Berwick, J., Kennerley, A.J., Mayhew, J.E.W., and Overton, P.G. (2012). Neurovascular coupling is brain region-dependent. *Neuroimage* 59, 1997–2006. <https://doi.org/10.1016/j.neuroimage.2011.09.050>.
31. Chen, Y., Cui, Q., Sheng, W., Tang, Q., Lu, F., Pang, Y., Nan, X., He, Z., Li, D., Lei, T., and Chen, H. (2021). Anomalous neurovascular coupling in patients with generalized anxiety disorder evaluated by combining cerebral blood flow and functional connectivity strength. *Prog. Neuro-Psychopharmacol. Biol. Psychiatry* 111, 110379. <https://doi.org/10.1016/j.pnpbp.2021.110379>.
32. Yabluchanskiy, A., Nyul-Toth, A., Csiszar, A., Gulej, R., Saunders, D., Towner, R., Turner, M., Zhao, Y., Abdelkari, D., Rypma, B., and Tarantini, S. (2021). Age-related alterations in the cerebrovasculature affect neurovascular coupling and BOLD fMRI responses: Insights from animal models of aging. *Psychophysiology* 58, e13718. <https://doi.org/10.1111/psyp.13718>.
33. Verriotes, M., Fabrizi, L., Lee, A., Cooper, R.J., Fitzgerald, M., and Meek, J. (2016). Mapping Cortical Responses to Somatosensory Stimuli in Human Infants with Simultaneous Near-Infrared Spectroscopy and Event-Related Potential Recording. *eNeuro* 3, ENEURO.0026-16.2016. <https://doi.org/10.1523/eneuro.0026-16.2016>.
34. Balconi, M., and Vanutelli, M.E. (2016). Hemodynamic (fNIRS) and EEG (N200) correlates of emotional inter-species interactions modulated by visual and auditory stimulation. *Sci. Rep.* 6, 23083. <https://doi.org/10.1038/srep23083>.
35. Huang, J., Wang, F., Ding, Y., Niu, H., Tian, F., Liu, H., and Song, Y. (2015). Predicting N2pc from anticipatory HbO activity during sustained visuospatial attention: A concurrent fNIRS-ERP study. *Neuroimage* 113, 225–234. <https://doi.org/10.1016/j.neuroimage.2015.03.044>.

36. Zhao, C., Li, D., Guo, J., Li, B., Kong, Y., Hu, Y., Du, B., Ding, Y., Li, X., Liu, H., and Song, Y. (2022). The neurovascular couplings between electrophysiological and hemodynamic activities in anticipatory selective attention. *Cereb. Cortex* 32, 4953–4968. <https://doi.org/10.1093/cercor/bhab525>.
37. Meltzer, J.A., Negishi, M., Mayes, L.C., and Constable, R.T. (2007). Individual differences in EEG theta and alpha dynamics during working memory correlate with fMRI responses across subjects. *Clin. Neurophysiol.* 118, 2419–2436. <https://doi.org/10.1016/j.clinph.2007.07.023>.
38. Adam, K.C.S., Robison, M.K., and Vogel, E.K. (2018). Contralateral Delay Activity Tracks Fluctuations in Working Memory Performance. *J. Cogn. Neurosci.* 30, 1229–1240. https://doi.org/10.1162/jocn_a.01233.
39. Robitaille, N., Marois, R., Todd, J., Grimault, S., Cheyne, D., and Jolicoeur, P. (2010). Distinguishing between lateralized and nonlateralized brain activity associated with visual short-term memory: fMRI, MEG, and EEG evidence from the same observers. *Neuroimage* 53, 1334–1345. <https://doi.org/10.1016/j.neuroimage.2010.07.027>.
40. Jensen, O., and Tesche, C.D. (2002). Frontal theta activity in humans increases with memory load in a working memory task. *Eur. J. Neurosci.* 15, 1395–1399. <https://doi.org/10.1046/j.1460-9568.2002.01975.x>.
41. Sauseng, P., Griesmayr, B., Frenzenberger, R., and Klimesch, W. (2010). Control mechanisms in working memory: A possible function of EEG theta oscillations. *Neurosci. Biobehav. Rev.* 34, 1015–1022. <https://doi.org/10.1016/j.neubiorev.2009.12.006>.
42. Chul, J., Tak, S., Jang, K.E., Jung, J., and Jang, J. (2009). NIRS-SPM: Statistical parametric mapping for near-infrared spectroscopy. *Neuroimage* 44, 428–447. <https://doi.org/10.1016/j.neuroimage.2008.08.036>.
43. Jaszewski, G., Strangman, G., Wagner, J., Kwong, K.K., Poldrack, R.A., and Boas, D.A. (2003). Differences in the hemodynamic response to event-related motor and visual paradigms as measured by near-infrared spectroscopy. *Neuroimage* 20, 479–488. [https://doi.org/10.1016/s1053-8119\(03\)00311-2](https://doi.org/10.1016/s1053-8119(03)00311-2).
44. Hakim, N., Adam, K.C.S., Gunseli, E., Awh, E., and Vogel, E.K. (2019). Dissecting the Neural Focus of Attention Reveals Distinct Processes for Spatial Attention and Object-Based Storage in Visual Working Memory. *Psychol. Sci.* 30, 526–540. <https://doi.org/10.1177/0956797619830384>.
45. Keles, H.O., Barbour, R.L., and Omurtag, A. (2016). Hemodynamic correlates of spontaneous neural activity measured by human whole-head resting state EEG plus fNIRS. *Neuroimage* 138, 76–87. <https://doi.org/10.1016/j.neuroimage.2016.05.058>.
46. Scheeringa, R., Petersson, K.M., Oostenveld, R., Norris, D.G., Hagoort, P., and Bastiaansen, M.C.M. (2009). Trial-by-trial coupling between EEG and BOLD identifies networks related to alpha and theta EEG power increases during working memory maintenance. *Neuroimage* 44, 1224–1238. <https://doi.org/10.1016/j.neuroimage.2008.08.041>.
47. Tomasi, D., Caparelli, E.C., Chang, L., and Ernst, T. (2005). fMRI-acoustic noise alters brain activation during working memory tasks. *Neuroimage* 27, 377–386. <https://doi.org/10.1016/j.neuroimage.2005.04.010>.
48. Lai, V., Theppitak, C., Makizuka, T., Higuchi, Y., Movahed, M., Kumudini, G., Izumi, H., and Kumashiro, M. (2014). A normal intensity level of psycho-physiological stress can benefit working memory performance at high load. *Int. J. Ind. Ergon.* 44, 362–367. <https://doi.org/10.1016/j.ergon.2013.11.015>.
49. Choe, J., Coffman, B.A., Bergstedt, D.T., Ziegler, M.D., and Phillips, M.E. (2016). Transcranial Direct Current Stimulation Modulates Neuronal Activity and Learning in Pilot Training. *Front. Hum. Neurosci.* 10, 34. <https://doi.org/10.3389/fnhum.2016.00034>.
50. Crone, N.E., Miglioretti, D.L., Gordon, B., Sieracki, J.M., Wilson, M.T., Uematsu, S., and Lesser, R.P. (1998). Functional mapping of human sensorimotor cortex with electrocorticographic spectral analysis - I. Alpha and beta event-related desynchronization. *Brain* 121, 2271–2299. <https://doi.org/10.1093/brain/121.12.2271>.
51. Liu, T.T., Frank, L.R., Wong, E.C., and Buxton, R.B. (2001). Detection power, estimation efficiency, and predictability in event-related fMRI. *Neuroimage* 13, 759–773. <https://doi.org/10.1006/nimj.2000.0728>.
52. Petersen, S.E., and Dubis, J.W. (2012). The mixed block/event-related design. *Neuroimage* 62, 1177–1184. <https://doi.org/10.1016/j.neuroimage.2011.09.084>.
53. Reinhart, R.M.G., and Nguyen, J.A. (2019). Working memory revived in older adults by synchronizing rhythmic brain circuits. *Nat. Neurosci.* 22, 820–827. <https://doi.org/10.1038/s41593-019-0371-x>.
54. Minamoto, T., Osaka, M., and Osaka, N. (2010). Individual differences in working memory capacity and distractor processing: Possible contribution of top-down inhibitory control. *Brain Res.* 1335, 63–73. <https://doi.org/10.1016/j.brainres.2010.03.088>.
55. Hsieh, L.T., Ekstrom, A.D., and Ranganath, C. (2011). Neural Oscillations Associated with Item and Temporal Order Maintenance in Working Memory. *J. Neurosci.* 31, 10803–10810. <https://doi.org/10.1523/jneurosci.0828-11.2011>.
56. Gao, Y., Liu, H., Fang, F., and Zhang, Y. (2023). Classification of Working Memory Loads via Assessing Broken Detailed Balance of EEG-fNIRS Neurovascular Coupling Measures. *IEEE Trans. Biomed. Eng.* 70, 877–887. <https://doi.org/10.1109/tbme.2022.3204718>.
57. Szczepanski, S.M., Crone, N.E., Kuperman, R.A., Auguste, K.I., Parvizi, J., and Knight, R.T. (2014). Dynamic Changes in Phase-Amplitude Coupling Facilitate Spatial Attention Control in Fronto-Parietal Cortex. *PLoS Biol.* 12, e1001936. <https://doi.org/10.1371/journal.pbio.1001936>.
58. Roy, Y., and Faubert, J. (2023). Is the Contralateral Delay Activity (CDA) a robust neural correlate for Visual Working Memory (VWM) tasks? A reproducibility study. *Psychophysiology* 60, e14180. <https://doi.org/10.1111/psyp.14180>.
59. Bentley, P., Husain, M., and Dolan, R.J. (2004). Effects of cholinergic enhancement on visual stimulation, spatial attention, and spatial working memory. *Neuron* 41, 969–982. [https://doi.org/10.1016/s0896-6273\(04\)00145-x](https://doi.org/10.1016/s0896-6273(04)00145-x).
60. Cutini, S., Scarpa, F., Scatturin, P., Jolicoeur, P., Pluchino, P., Zorzi, M., and Dell'Acqua, R. (2011). A hemodynamic correlate of lateralized visual short-term memories. *Neuropsychologia* 49, 1611–1621. <https://doi.org/10.1016/j.neuropsychologia.2010.12.009>.
61. Scarpa, F., Cutini, S., Scatturin, P., Dell'Acqua, R., and Sparacino, G. (2010). Bayesian filtering of human brain hemodynamic activity elicited by visual short-term maintenance recorded through functional near-infrared spectroscopy (fNIRS). *Opt Express* 18, 26550–26568. <https://doi.org/10.1364/oe.18.026550>.
62. Akyürek, E.G., Vallines, I., Lin, E.J., and Schubö, A. (2010). Distraction and target selection in the brain: An fMRI study. *Neuropsychologia* 48, 3335–3342. <https://doi.org/10.1016/j.neuropsychologia.2010.07.019>.
63. Nobre, A.C., and van Ede, F. (2023). Attention in flux. *Neuron* 111, 971–986. <https://doi.org/10.1016/j.neuron.2023.02.032>.
64. Esterman, M., and Rothlein, D. (2019). Models of sustained attention. *Curr. Opin. Psychol.* 29, 174–180. <https://doi.org/10.1016/j.copsyc.2019.03.005>.
65. Yeung, M.K., and Chu, V.W. (2022). Viewing neurovascular coupling through the lens of combined EEG-fNIRS: A systematic review of current methods. *Psychophysiology* 59, e14054. <https://doi.org/10.1111/psyp.14054>.
66. Huo, B.X., Smith, J.B., and Drew, P.J. (2014). Neurovascular Coupling and Decoupling in the Cortex during Voluntary Locomotion. *J. Neurosci.* 34, 10975–10981. <https://doi.org/10.1523/jneurosci.1369-14.2014>.
67. Schaeffer, S., and Iadecola, C. (2021). Revisiting the neurovascular unit. *Nat. Neurosci.* 24, 1198–1209. <https://doi.org/10.1038/s41593-021-00904-7>.
68. Li, R., Potter, T., Huang, W., and Zhang, Y. (2017). Enhancing Performance of a Hybrid EEG-fNIRS System Using Channel Selection and Early Temporal Features. *Front. Hum. Neurosci.* 11, 462. <https://doi.org/10.3389/fnhum.2017.00462>.
69. Button, K.S., Ioannidis, J.P.A., Mokrysz, C., Nosek, B.A., Flint, J., Robinson, E.S.J., and Munafò, M.R. (2013). Confidence and precision increase with high statistical power. *Nat. Rev. Neurosci.* 14, 585–586. <https://doi.org/10.1038/nrn3475-c4>.
70. Delorme, A., and Makeig, S. (2004). EEGLAB: an open source toolbox for analysis of single-trial EEG dynamics including independent component analysis. *J. Neurosci. Methods* 134, 9–21. <https://doi.org/10.1016/j.jneumeth.2003.10.009>.
71. Cui, X., Bray, S., and Reiss, A.L. (2010). Functional near infrared spectroscopy (NIRS) signal improvement based on negative correlation between oxygenated and deoxygenated hemoglobin dynamics. *Neuroimage* 49, 3039–3046. <https://doi.org/10.1016/j.neuroimage.2009.11.050>.
72. Li, D., Zhao, C., Guo, J., Kong, Y., Li, H., Du, B., Ding, Y., and Song, Y. (2021). Visual Working Memory Guides Spatial Attention: Evidence from alpha oscillations and sustained potentials. *Neuropsychologia* 151, 107719. <https://doi.org/10.1016/j.neuropsychologia.2020.107719>.

STAR★METHODS

KEY RESOURCES TABLE

REAGENT or RESOURCE	SOURCE	IDENTIFIER
Deposited data		
Data used in this paper	This paper	https://doi.org/10.17605/OSF.IO/98Q3F
Software and algorithms		
MATLAB R2020b	MathWorks	http://www.mathworks.com/products/matlab/
CURRY 8.0	Compumedics Neuroscan	https://compumedicsneuroscan.com/products/by-name/curry/
Psychtoolbox-3	N/A	http://psychtoolbox.org/
EEGLAB	N/A	http://sccn.ucsd.edu/eeglab/index.html
JASP 0.9.2.0	JASP	https://jasp-stats.org/
NIRS-SPM	Korea Advanced Institute of Science and Technology	http://bisp.kaist.ac.kr/NIRS-SPM
Other		
EEG	Neuroscan	N/A
fNIRS	Hitachi ETG-4000	N/A
Code used in this paper	This paper	https://doi.org/10.17605/OSF.IO/98Q3F

RESOURCE AVAILABILITY

Lead contact

Further information and requests for resources and results should be directed to the lead contact Chenguang Zhao (chenguang918.zhao@gmail.com).

Materials availability

This study did not generate new unique reagents.

Data and code availability

- All EEG and fNIRS raw data have been deposited at Open Science Framework (OSF) and are publicly available as of the date of publication. The DOI is listed in the [key resources table](#).
- All original code has been deposited at OSF and is publicly available as of the date of publication. DOI is listed in the [key resources table](#).
- Any additional information required to reanalyze the data reported in this paper is available from the [lead contact](#) upon request.

EXPERIMENTAL MODEL AND STUDY PARTICIPANT DETAILS

Thirty-five participants (21 females and 14 males; age range 18.2–27.1 years, mean age 24.5 years; all Asians) who were all right-handed and had normal or corrected normal vision were included in our experiment. Gender, ancestry, and ethnicity were not considered in the study as there was no evidence that vWM task could be biased by those parameters. Seven participants were excluded because of incomplete data or low signal quality. The experimental procedures of the study were approved by the Institutional Review Board of Beijing Normal University. Each participant signed an informed consent form.

METHOD DETAILS

Working memory task

The visual stimuli were displayed on a 20-inch CRT monitor with 1600 × 900 pixels and a refresh rate of 120 Hz and placed 60 cm from the participant. As shown in [Figure 1A](#), the participants were instructed to keep their eyes fixed on the cross in the center of the screen throughout the experiment. A spatial arrow cue was presented at the beginning of each trial for 200 ms, instructing the participants to remember items that appeared in the left or right semifiel. Next, memory items with a homogeneous light gray background (12 cd/m², RGB: 125, 125, 125) were presented for 100 ms, followed by a 900 ms delay with a blank display. Finally, the probe display was presented until a response was given or after a maximum time of 2000 ms, and participants were required to quickly and accurately determine whether the orientation of the items that appeared in the cued hemifiel had changed in the test display.

All memory items were nonoverlapping and randomly distributed within the bilateral rectangular regions ($4^\circ \times 7.3^\circ$) centered 3° on both sides of a black central fixation point (0.5 cd/m^2 , $0.4^\circ \times 0.4^\circ$). The distance between the center and the centers of the bars within a hemifield was at least 2° . Each memory display comprised two or four $2^\circ \times 0.5^\circ$ red bars with random orientations between 0° and 180° . The orientations of the bars within the hemifield differed by at least 20° . In 50% of the trials, the items on the test display were the same as those used for the memory display. In the remaining 50% of trials, the orientation of one bar in the test display was changed by at least 15° from that of the corresponding items in the memory display. In the baseline condition, the two red bars were presented in each hemisphere. In the scope-increased condition, an increase of the four red bars was presented in each hemisphere. In the control-increased condition (2T2D), the two red and two blue bars were presented in each hemisphere.

Miniblock nesting rest state design

Each experimental condition consisted of three blocks with randomization applied across blocks. Each block was separated at approximately 30 s intervals. Within each block, there were six miniblocks, each separated by a 10 s rest period. The 10 s closed-eye resting state was interleaved between the miniblocks to speed up the return of the hemodynamic signal and prevent a temporal overlap of the prior hemodynamic response. A simple illustration in Figure 5A shows that the ΔHbO concentration was reduced to the prior baseline after recovery of the closed-eye resting state (see Figures S3 and S4 for details).

Participants closed their eyes when the fixation disappeared. The participants were asked to open their eyes after hearing the onset beep, then a 2.2 s countdown allowed them to prepare for the upcoming stimulus (Figure 1C). Every miniblock encompassed 12 trials, wherein participants were presented with randomly occurring memory tasks involving stimuli moving either left or right. Participants were required to discern the congruence of the presented stimuli based on cue indications and respond promptly using a keypress. Consequently, each unique experimental condition comprised 3 blocks \times 36 miniblocks \times 12 trials (1296 trials). The entire experimental session was extended to approximately 50 min.

In traditional block-based experimental designs, the issue of overlapped blood oxygenation response signals often arises, leading to a reduction in the interpretative efficiency of the GLM. This occurs due to the classical hemodynamic response function being based on an ideal model of short-term, single-event responses. The aim was to facilitate a rapid return of blood oxygenation signals to a consistently lower level, effectively mitigating mutual interference among miniblocks caused by continuous stimuli.

Resting period effectiveness

As illustrated in Figure S3 left, the mean values of all channels are depicted for three different conditions, and the HbO variations during the resting phase exhibited a remarkably consistent trend. Following the conclusion of each miniblock, an immediate transition into a closed-eye resting state occurs. The ΔHbO signal exhibits a distinctive pattern: a gradual rise, reaching its peak at approximately 6 s, followed by a rapid decline until the onset of the eye-opening event. After reaching its peak following the peak of the ΔHbO signal and before the occurrence of the open-eye event, the statistical results within this timeframe demonstrated a significant decreasing trend in the ΔHbO signal, as illustrated in Figure S3 right. The above results indicated that introducing brief periods of rest indeed accelerates the signal decline and restores the baseline at a global level.

To validate the effectiveness of the added resting period, not only in expediting signal recovery but also in enhancing the interpretability of the GLM, thereby bolstering the credibility of the results, we performed GLM estimations using distinct predictors (design matrices), as illustrated in Figures S4A–S4C. We conducted three identical GLM estimations on all data sets, with the sole difference being the design matrix employed.

$$y_{\text{HbO}} = (\delta_i \otimes \text{HRF})\beta_i + \epsilon_{\text{Res}} \quad (\text{Equation 1})$$

y_{HbO} is the signal for changes in blood oxygen concentration. β_i are time series associated with different event conditions, where $i=1$ including only the task time; $i=2$ adding rest events: adding random event. β_i corresponds to regression coefficients for different event combinations. ϵ_{Res} is the residual term, and its standard deviation (SD) can reflect the explanatory power of the GLM, a lower SD indicating that the model fits the data better.

The first design matrix exclusively encompassed stimulus events; the second incorporated resting events; and the third introduced a series of random events. The metric was defined as the mean residual error (MRE) of the GLMs. MRE indicated the goodness of fitting between the expected model and the actual measured data. A smaller MRE would therefore represent a better fitting of the linear model. The residual statistics presented in Figure S4D indicate that there is no significant difference in GLM residuals between task events and the addition of random events. However, the incorporation of resting events significantly reduces the residuals of the GLM fit compared to both scenarios. This to some extent suggested that adding resting periods indeed improves the model's explanatory capacity.

Furthermore, we investigated dispersion parameters and obtained corroborating results. Our findings from a model interpretative standpoint affirm our hypothesis that a miniblock-based experimental design effectively mitigates the interference stemming from overlapped consecutive stimulus events. This study contributes valuable insights toward refining the experimental design for enhanced accuracy in data interpretation.

Simultaneous data acquisition

Simultaneous EEG and fNIRS signals were recorded while the participants performed all tasks. The EEG data were recorded using a SynAmps2 amplifier and the Curry 8.0 package (Compumedics Neuroscan, USA). The fNIRS signals were recorded using an ETG-4000 system at 830 nm and 695 nm (Hitachi Medical, Japan). Thirty-two Ag-AgCl electrodes from the EEG cap were arranged according to the international 10–20 system. Four additional facial electrodes were placed at the outer canthi and 1 cm above and below the left eye to record the horizontal or vertical electrooculogram (EOG) data, and two electrodes were placed at the left and right mastoids. A 46-channel fNIRS measurement using one 3 × 5 and two 3 × 3 optode probe sets covered the PFC and PPC (Figure 1D). The fNIRS signals acquired at 10 Hz and EEG signals acquired at 1000 Hz were synchronized using an external event-triggered marker generated by Psychtoolbox-3 (<http://psychtoolbox.org>) from Matlab. A linear correction was applied to the timeline of the data using the relative time of identical markers, resulting in a synchronization error of less than 0.1 s. For online EEG recording, electrode impedances were maintained below 5 kΩ for all remaining electrodes. The EEG data were digitized online, and a bandpass filter of 0.01–200 Hz was applied.

Preprocessing

Preprocessing was performed using functions extracted from EEGLAB.⁷⁰ The EEG signals were 0.1–40 Hz bandpass filtered and referenced to the average of the left and right mastoids. The filtered EEG data were decomposed into independent components using the independent component analysis (ICA) algorithm. One or two components that showed the highest correlation with vertical EOG (eye blink) were removed. The EEG data were then segmented from 500 ms to 1200 ms for memory display. EEG epochs exceeding ±100 μV at any electrode or horizontal EOG exceeding ±30 μV were automatically excluded from 0 ms to 500 ms around memory display onset. Data from four participants with a high proportion (>40%) of excluded trials were excluded from the final dataset. An average of 12.1 ± 6.7% of trials per participant were rejected due to artifacts.

For offline NIRS data processing and analyses, light intensity changes were converted to the concentration changes in deoxy- and oxyhemoglobin (ΔHbR and ΔHbO) according to the modified Beer-Lambert law. Bad channels were detected and interpolated using adjacent channel data. Channels with the following conditions were marked as bad channels: (1) the coefficient of variation (CV) deviated from the average value by more than 90%; (2) the correlation coefficient between ΔHbO and ΔHbR was not significant; and (3) the power spectrum of the fNIRS signal did not show a significant peak in the heart rate component. Approximately 10% of the total number of channels was marked in all subjects. The raw data were preprocessed by applying a bandpass filter with cutoff frequencies of 0.01–0.2 Hz. Motion artifacts were corrected using a correlation-based signal improvement algorithm.⁷¹

Behavior analysis

Trials with reaction times exceeding the threshold range (less than 0.4 s or greater than 1.5 s) were excluded from the analysis. Control and scope attention scores during vWM were calculated using the following formulas:

$$\text{Attention control score} = 2 + (K_{2T2D} - K_{2T}) \quad (\text{Equation 2})$$

$$\text{Attention scope score} = \max \{K_{2T}, K_{4T}\} \quad (\text{Equation 3})$$

The dynamic K value was computed for the tth miniblock of the entire task using the following formula:

$$K(t) = N(t) \times (H(t) - F(t)) \quad (\text{Equation 4})$$

Where N is the set size of the tth miniblock, t is the serial number of the miniblock, H(t) is the observed hit rate of the tth miniblock, and F(t) is the false alarm rate of the tth miniblock. The use of such formulas is based on the premise that, during a certain period, an individual has a stable ability to hold K items from an array of N items in vWM, which leads to correct performance on K/N in the trials.

ERP analysis

We focused on the CDA component induced by the memory display. The baseline correction was calculated by subtracting the mean signal within the prior 200 ms to memory display onset. ERP waveforms were created by averaging all trials for the six conditions (two visual hemifields × three experimental conditions). To isolate the CDA difference waves from the nonlateralized ERPs, the waveforms at electrodes P3/4 and P7/8, ipsilateral to the side of the items to be remembered, were subtracted from the contralateral ERPs. In this task, a memory display can induce a lateralized N2 posterior contralateral (N2pc) before the CDA component.⁷² To measure the CDA amplitude alone without N2pc contamination, the detection window started from 500 ms, when N2pc had ordinarily terminated.

During ERP analysis for the two WM characteristics, the difference in CDA between baseline (2T) and scope-increased conditions (4T) was calculated as the WM scope with t-statistical analysis. The differences between baseline (2T) and control-increased (2T2D) conditions were used to identify WM control processes. For each comparison, a test was performed at each time point with random permutations (N = 1000). Our electrodes of interest were the bilateral occipitoparietal electrodes (P3/4 and P7/8), based on previous findings.²⁴

EEG oscillation

For the EEG oscillation analysis, artifact-free trials were transformed using Morlet wavelet decomposition in 1 Hz steps. Subsequently, to calculate the induced neural oscillation responses without the evoked potential mask, the trial-averaged ERPs in the time domain were subtracted from the raw EEG signals on a trial-by-trial basis. Theta power changes (4–7 Hz) during retention were calculated to examine the scope-related oscillatory activity between the baseline (2T) and scope-increased conditions (4T). Changes in control-dependent oscillatory activity were calculated to examine the difference between the baseline (2T) and control-increased conditions (2T2D). The theta band ERS measures were in line with the procedure reported^{25,26} as follows: 1) the reference interval (400–0 ms) before memory display onset was subtracted from the power estimates at each time point, and 2) the difference was divided by the reference interval. Changes in baseline over time are referred to as ERS. The electrodes of interest were the middle frontal electrodes (FP1/2, F3/4, F1/2, and FZ).

General linear model

We used a GLM to analyze the hemodynamic response functions (HRFs) for different stimuli.

$$Y_{\text{fNIRS}} = X_{\text{Rest}}\beta_0 + X_{\text{Stim}}\beta_1 + \varepsilon \quad (\text{Equation 5})$$

Where Y_{fNIRS} is the time series of the fNIRS signal, β_1 is the regression coefficient, and ε is the error term. The design matrix X_{Stim} is a convolution of the stimulus sequence, X_{Rest} is a convolution of the active rest-state sequence and basis functions, and uses the same bandpass filter as that used for preprocessing. The basis functions are a set of Gaussian functions with widths of 2 s and steps of 2 s. Therefore, HRF can be estimated using the following formula:

$$\text{HRF}_{\text{estimated}} = \sum \Phi_{\tau}\beta_{\tau} \quad (\text{Equation 6})$$

Where Φ_{τ} are the Gaussian basis functions and β_{τ} are regression coefficients associated with each basis function, with τ representing the time delay (–2–8 s).

Task-related activation

To evaluate the activation strength of hemodynamic activity under various conditions, a design matrix was constructed by convolving cue events with a sequence of basis functions. These pivotal cue events prompted participants to actively engage in a cognitive task in which they were required to memorize the visual content of stimuli occupying precisely half of the screen's spatial area as directed by arrow cues. The cue events marked critical moments in the experimental protocol, representing instances in which the participants were prompted to shift their attention and encode specific visual information. The basis functions were a series of Gaussian functions with a width of 2 s and a step size of 2 s. GLM analysis was then used to assess the hemodynamic activation levels.

A t-test was conducted to identify the channels that rejected the null hypothesis $\beta_{4T} = \beta_{2T}$ or $\beta_{2T} = \beta_{2T2D}$ ($p < 0.05$):

$$t = \frac{c^T \Delta \hat{\beta}}{\sqrt{\hat{\sigma}^2 c^T (X^T X)^{-1} c}} \quad (\text{Equation 7})$$

Where the estimate of weights $\Delta \hat{\beta} = \beta_{4T} - \beta_{2T}$ or $\beta_{2T2D} - \beta_{2T}$, $\hat{\sigma}^2$ is the residual sum-of-squares divided by the degrees of freedom, c is the channel vector.

Hemodynamic contralateral delay activity

To conduct an analysis similar to the typical approach in CDA involving a lateralized analysis, we compared each channel of one hemisphere with its corresponding symmetrical channel in the opposite hemisphere. The initial step involved separately fitting and estimating the hemodynamic responses to stimulus events on both the same and opposite sides. Subsequently, the relative changes in blood oxygen concentration (hemodynamic CDA) were obtained by subtracting the hemodynamic response on the ipsilateral side from the corresponding channel response on the contralateral side.

EEG-informed analysis

In the present study, the design matrix contained three modeled hemodynamic response functions corresponding to X_{Stim} , X_{EEG} , and X_{Rest} . To find NVC results that were specifically related to the EEG features and not to some general features of the stimulus events, we used Schmidt-Gram orthogonalization. The orthogonalized sequences were then convolved with a standardized hemodynamic response function (HRF) convolved with a canonical hemodynamic response function, and subsequently modeled using GLM to establish a linear relationship between EEG features and ΔHbO features.

$$Y_{\text{fNIRS}} = X_{\text{Rest}}\beta_0 + X_{\text{Stim}}\beta_1 + X_{\text{EEG}}\beta_{\text{NVC}} + \varepsilon \quad (\text{Equation 8})$$

Where $y_{\Delta\text{HbO}}$ is the sequences of the ΔHbO features, X_{EEG} is the design matrix of EEG features, β_{NVC} is the regression coefficients to estimate NVC strengths, and ε is the error term. X_{Stim} was orthogonalized with respect to X_{EEG} by removing the part of X_{Stim} that was correlated to X_{EEG} .

The EEG-informed NVC (theta-informed or CDA-informed) features were used as the regressor and the dynamic K value was used under different conditions as the data to be regressed for each individual (see the pipeline in [Figure 5A](#)). To visualize our results, we plotted a coefficient brain map with a statistical t-value at a typical threshold FDR value ($p < 0.05$) (see [Figure 5B](#)).

Modeling analysis

To assess the relationship between dynamic behavior and dynamic NVC in miniblocks at the group level, a linear mixed model was used with NVC as a predictor and the K value as a response variable. Separate models were fit for each channel and estimates for group-level fixed effects (β_1), intercepts (β_0), and random effects (b_{0i} , b_{1i}) were obtained.

Because the K value on the 1st miniblock and the relationship between dynamic K and dynamic NVC may vary for each patient, a random intercept (b_{0i}) and a slope (b_{1i}) were used.

$$K_{ij} = \beta_0 + \beta_1 \text{NVC}_{ij} + b_{0i} + b_{1i} \text{NVC}_{ij} + \epsilon_{ij} \quad (\text{Equation 9})$$

Where b_{0i} and b_{1i} are random intercepts and slopes for subject i , and $b_{0i} \sim N(0, \tau^2)$, $b_{1i} \sim N(0, \tau_{1i}^2)$, and K_{ij} denotes the j th fNIRS channel for subject i , NVC_{ij} indexes the EEG-informed NVC from j channel for subject i . ANOVA identified the relationship between dynamic K and dynamic NVC, and significant main effects of NVC were reported after adjusting for a FDR of 0.05. The t-statistic was used to determine the significance of the ROI across the whole-brain map.

QUANTIFICATION AND STATISTICAL ANALYSIS

Bayes factor analyses with default priors ($r = 0.707$) were performed on fNIRS and EEG data. Bayesian analysis was conducted using JASP software v. 0.9.2.0 to test the null hypothesis ($\text{BF}_{10} < 0.333$: substantial evidence for the null hypothesis; $\text{BF}_{10} > 1$: support for H1 over H0).

ROC analysis was performed for the GLM binomial model. Each model was used to predict the attention performance based on EEG, ΔHbO , and NVC metrics for each miniblock at a single subject level. We calculated the false positive rate (FPR, 1-specificity) and true positive rate (TPR, sensitivity) and generated the ROC curve by varying the p-value threshold (0 to 1). The AUC of the ROC can be calculated to quantify the overall performance of each model. A higher AUC indicates that the model performs better in predicting the behavior. To compare the performance of different models, a one-way repeated ANOVA test was employed to evaluate the difference in these metrics among the models based on EEG, ΔHbO , and NVC metrics.

ADDITIONAL RESOURCES

This paper did not create any additional resources.